Cellular/Molecular

Nonrandom Local Circuits in the Dentate Gyrus

Phillip Larimer and Ben W. Strowbridge
Department of Neurosciences, Case Western Reserve University, Cleveland, Ohio 44106

The dentate hilus has been extensively studied in relation to its potential role in memory and in temporal lobe epilepsy. Little is known, however, about the synapses formed between the two major cell types in this region, glutamatergic mossy cells and hilar interneurons, or the organization of local circuits involving these cells. Using triple and quadruple simultaneous intracellular recordings in rat hippocampal slices, we find that mossy cells evoke EPSPs with high failure rates onto hilar neurons. Mossy cells show profound synapse specificity; 87.5% of their intralamellar connections are onto hilar interneurons. Hilar interneurons also show synapse specificity and preferentially inhibit mossy cells; 81% of inhibitory hilar synapses are onto mossy cells. Hilar IPSPs have low failure rates, are blocked by the $GABA_A$ receptor antagonist gabazine, and exhibit short-term depression when tested at 17 Hz. Surprisingly, more than half (57%) of the mossy cell synapses we found onto interneurons were part of reciprocal excitatory/inhibitory local circuit motifs. Neither the high degree of target cell specificity, nor the significant enrichment of structured polysynaptic local circuit motifs, could be explained by nonrandom sampling or somatic proximity. Intralamellar hilar synapses appear to function primarily by integrating synchronous inputs and presynaptic burst discharges, allowing hilar cells to respond over a large dynamic range of input strengths. The reciprocal mossy cell/interneuron local circuit motifs we find enriched in the hilus may generate sparse neural representations involved in hippocampal memory operations.

Key words: **dentate gyrus; EPSP; IPSP; short-term plasticity; paired-recording; local circuits; two-photon imaging**

Introduction

The computations performed by brain regions directly reflect the organization of local circuits. To understand how these local circuits function, it is necessary to define both the organization of monosynaptic connections and how individual connections are integrated into polysynaptic networks. Local circuit structure can vary from random to iterated stereotyped networks. No previous studies have identified nonrandom polysynaptic local circuits that are statistically enriched in the hippocampus, although computer modeling studies have highlighted their potential importance (Klemm and Bornholdt, 2005; Morgan and Soltesz, 2008). Deciphering the neural computations in the hippocampus, including those involved in memory formation, is predicated on understanding the organization of polysynaptic circuits in this region.

The dentate hilus (see Fig. 1*A*) is an attractive brain region to examine the organization of hippocampal local circuits. Unlike most cortical areas, hilar interneurons and principal neurons [glutamatergic mossy cells (MCs)] exist in similar numbers (Buckmaster and Jongen-Rêlo, 1999), potentially enabling highly complex local networks. Mossy cells, unlike the more prevalent granule cells, project widely through the septo-temporal axis of the hippocampus (Buckmaster et al., 1996). Presumably the neural computation performed on granule cell inputs by hilar circuitry determines what information is transmitted to other hippocampal lamellae. Consistent with this hypothesis, the hilus has been implicated in both memory dysfunction (Sass et al., 1992) and in temporal lobe epilepsy (Sloviter, 1987). The correlation of hilar cell loss with memory deficits in epileptic patients (Sass et al., 1992) suggests that mossy cells may play a critical role in hippocampal memory.

Only two studies have reported synaptic responses made by hilar cells. Scharfman (1995) showed that trains of action potentials (APs) in a mossy cell can trigger depolarizations in other dentate neurons. There are no published reports of inhibitory synapses between pairs of hilar neurons, although the same group also reported (Scharfman et al., 1990) slow depolarizations in mossy cells after bursts of APs in hilar interneurons. No data exist on the functional properties of hilar synapses and the organization of local circuits in the hilus. The paucity of physiological data on hilar local circuits contrasts with the wealth of anatomical reports that support the existence of asymmetric synapses from mossy cells to hilar interneurons (Buckmaster et al., 1996) and mossy cells (Wenzel et al., 1997) as well as symmetric synapses made by interneurons onto mossy cells (Halasy and Somogyi, 1993). Anatomical studies suggest that hilar neurons are highly interconnected (Sik et al., 1997; Wenzel et al., 1997; Katona et al., 1999) but cannot reveal the organization or function of polysynaptic circuits.

One difficulty in defining hilar circuitry physiologically is the high frequency of spontaneous synaptic inputs onto hilar cells (Scharfman, 1993; Strowbridge and Schwartzkroin, 1996). Analyzing responses to imprecisely timed trains of presynaptic APs, as in previous studies (Scharfman et al., 1990; Scharfman, 1995),

Received July 31, 2008; revised Sept. 17, 2008; accepted Oct. 6, 2008.

This work was supported by National Institutes of Health (NIH) Grant R01-NS33590 to B.W.S. P.L. was supported by NIH Grant T32-AG00271. We thank Drs. Roberto Galan, Jason Frazier, and Phil Williams for their constructive comments on this manuscript.

Correspondence should be addressed to Dr. Ben W. Strowbridge, Department of Neurosciences, Case Western Reserve University, 10900 Euclid Avenue, Cleveland, OH 44106. E-mail: bens@case.edu.

DOI:10.1523/JNEUROSCI.3612-08.2008

 0270-6474/08/2812212-12$15.00/0

may be confounded by correlated synaptic input. In this study, we used numerous (>200) repetitions of precisely timed presynaptic action potentials in simultaneous two-, three-, and four-hilar cell recordings to define for the first time the properties of hilar synapses and the most common local circuits in the hilus. We find that mossy cells and hilar interneurons exhibit pronounced target cell type specificity and are interconnected through reciprocal synapses at frequencies significantly higher than expected.

Materials and Methods

Recording methods. Horizontal slices (300 μm thick) were prepared from the ventral rat hippocampi of 14- to 21-d-old Sprague Dawley rats using a modified Leica VT1000S vibratome. All recordings were performed in a submerged recording chamber mounted to the stage of an upright microscope (Zeiss Axioskop 1 FS). Slices were maintained at 30°C and perfused at ~2 ml/min with standard artificial CSF (ACSF) that contained (in mM): 124 NaCl, 3 KCl, 1.23 NaH_2PO_4, 1.2 $MgSO_4$, 26 $NaHCO_3$, 10 dextrose, and 2.5 $CaCl_2$ equilibrated with 95% O_2/5% CO_2, as described previously (Frazier et al., 2003; Williams et al., 2007). Whole-cell current clamp recordings were made using an internal solution that contained (in mM): 140 K methylsulfate, 4 NaCl, 10 HEPES, 0.2 EGTA, 4 MgATP, 0.3 Na_3GTP, 10 phosphocreatine (290 mOsm; pH 7.3). Neurons were visualized using infrared differential interference contrast (IR-DIC) optics. We did not attempt to quantify aspects of neuronal morphology using IR-DIC microscopy because of the limited ability of this method to visualize fine detail in acute brain slices.

Between two and four hilar cells located within the field-of-view of a 63× water-immersion objective (80 μm) were recorded simultaneously using Axopatch 1D amplifiers (Molecular Devices) and tested for synaptic interactions using staggered sets of short-duration (10 ms) depolarizing current steps. We did not systematically test for electrical coupling between pairs of hilar cells in this study. However, we observed one example (of 251 possible pairings) with obvious electrical coupling associated with action potential bursts. We confirmed electrical coupling in this example (a paired recording between two hilar interneurons) by injecting hyperpolarizing current pulses and estimated the coupling ratio to be 18%.

All neurons were at least 80 μm from the granule cell layer, in the "deep" hilus, to preclude recording from basket cell and ectopic granule cells in the subgranular zone. Mossy cells constituted 65% of our data set, in accordance with the ratio of mossy cells to hilar interneurons based on GAD immunohistochemistry (64% mossy cells) Buckmaster and Jongen-Rêlo, 1999; Amaral, 1978). The close correlation between the percentage of mossy cells in our study and anatomical estimates of the ratio of hilar neuron subtypes suggests that our recordings sampled randomly from deep hilar neurons. We recorded from three to four hilar neurons simultaneously in one slice in most experiments. The high incidence of overlapping neurites from these multipolar neurons precluded using intracellular dyes to visualize neuronal morphology while searching for monosynaptic connections. Instead, we recorded from a second group of hilar neurons using patch clamp electrodes containing 100 μM Alexa488 hydrazide (Invitrogen). The intrinsic physiological properties of these neurons were then analyzed and correlated with morphological properties visualized using two-photon microscopy. Morphometric parameters were calculated from maximal Z-stack projections acquired from living slices. Shape factor was defined as the ratio between the two largest orthogonal axes. Cell body area was estimated by approximating this region as an ellipse ($(\pi/4)$ * length * width). In most cases, cell body regions of filled hilar neurons varied from ellipsoid to triangular.

Voltage records were low-pass filtered at 2 kHz (FLA-1, Cygnus Technology) and sampled at 5 kHz using a 16-bit analog-to-digital converter (ITC-18, Instrutech). Data were acquired and analyzed with custom software written in Matlab (Mathworks). Voltages presented are not corrected for the liquid junction potential [approximately −10 mV as calculated by JPCalc (Axon Instruments)]. The estimated Cl^- equilibrium potential was −91 mV (−81 mV when adjusted for the liquid junction potential in our recordings). Except where noted, statistical significance was determined using Student's *t* test. Multiple comparisons of different intrinsic properties were Bonferroni corrected. Data are presented as mean ± SEM.

Analysis of intrinsic properties. Input resistance was calculated from steady-state responses to weak hyperpolarizing steps (~10 mV amplitude); membrane time constant was calculated from single exponential fits to the initial phases of these responses. Spike-evoked afterhyperpolarizations (AHPs) were quantified by determining the decay-phase slope for 12 ms after the maximal AHP. The propensity of some hilar neurons to fire more frequently during the initial response to depolarizing steps was estimated by calculating the mean spike time for all APs evoked by a depolarizing step; step duration of 4.6 s normalized to 1. All steps used to classify hilar neurons were from −70 mV. Initial membrane potentials reported in figures were maintained with a constant bias current; synaptic responses typically were recorded between −55 and −60 mV to enable EPSPs and IPSPs to be differentiated. Mossy cells rested at −63.7 ± 1.7 mV and hilar interneurons rested at −57.8 ± 4.3 mV with no added bias current. We also defined the "spike clustering fraction" (Dekhuijzen and Bagust, 1996) as the fraction of APs that followed, or preceded, another AP by <60 ms. We calculated the individual metrics from responses to at least 3 current steps; reported values are the median of each metric for spike AHP and mean spike time and the maximum for the spike clustering fraction. The separation plane used to categorize hilar neurons (see Fig. 3*C*) had almost equal weighting of two spike timing metrics (spike clustering fraction and mean spike time) and a lesser contribution from the AHP slope component and used an equation in general form: $0.695X + 0.661Y + 0.284Z - 0.859 = 0$.

Distance to the plane is given by substitution of X,Y, and Z with values for mean spike time, spike clustering fraction, and AHP slope, respectively. The distance metric reported was the natural log of this distance; negative distance metrics represent points above the plane (hilar interneurons) whereas positive metrics represent points below the plane (mossy cells). The position of the separation plane was constrained to be between the two clusters; the exact position was determined by maximizing a summed exponential distance of each point from the plane using the Levenberg-Marquardt least-squares algorithm implemented within Matlab. The coefficients of the alternate plane calculated using linear discriminant analysis were: 0.764, 0.661, 0.180, and −0.889.

Analysis of synaptic potentials. We implemented an automated search strategy using Matlab to identify monosynaptic excitatory and inhibitory connections in a background of frequent spontaneous inputs. Monosynaptic excitatory potentials were designated by threshold crossings on a cumulative derivative plot, adapted from a previously published method (Cohen and Miles, 2000). We calculated the instantaneous derivative from a smoothed voltage trace (moving average, 1 ms window). The resulting intermediate trace was also smoothed (second-order Savitsky-Golay filter, 1.4 ms window) to increase sensitivity. Finally, we generated a third trace that reflected only positive-going events in the original signal by integrating positive derivatives and resetting on negative derivatives (i.e., an "up-only" cumulative derivative function). Events were defined by when the cumulative dV/dt exceeded 0.1 mV. Monosynaptic IPSPs were identified using an inverse version of the cumulative dV/dt method above.

For each potential connection, we first estimated the expected frequency of successes based on the number of PSPs detected in ~40 control windows (3 ms duration) in >100 episodes. This estimate was compared with the frequency of PSPs detected immediately after evoked presynaptic APs (onset latencies between 0.6 and 3.6 ms) in the same episodes. A χ^2 test was used to determine whether the spontaneous PSP rate was sufficient to account for the number of PSPs that followed presynaptic APs. All synaptic connections presented in this study were highly significant using this test ($p < 0.001$; average of 260 responses tested per connection). The actual number of control windows analyzed was slightly <40 for several connections because some windows were rejected because of spontaneous spiking in the presynaptic cell. We also generated mean voltage traces to confirm each excitatory and inhibitory connection identified by the automated method and to search for any missed connections. Mean voltage traces were calculated by averaging 100–150 spike-aligned episodes and then ranking these traces based on the mean

voltage difference in a 10–16 ms window after the presynaptic action potential from a baseline window.

Both derivative- and average trace-based search methods identified the same population of 9 excitatory and 22 inhibitory monosynaptic connections in our data set. The monosynaptic inhibitory connections we identified met the following criteria: (1) synaptic response $>50\ \mu V$ on the average voltage trace, (2) statistically significant increase in IPSP frequency in the time window immediately after the presynaptic AP ($p < 0.0001$ on the χ^2 test described above), and (3) >20 visually confirmed IPSPs with monoexponential rising phases that began during the test window. The monosynaptic excitatory connections we identified satisfied the same three tests, but with slightly different thresholds ($p < 0.001$ on the χ^2 test, ≥10 visually confirmed PSPs with monoexponential rising phases), reflecting the higher failure rates of excitatory connections. The population of monosynaptic connections analyzed for the phenotype of the postsynaptic neuron was slightly smaller (8 excitatory and 21 inhibitory connections) than the total number of identified connections because of a group of corrupted data files containing responses to 4.6 s duration depolarizing steps used to classify postsynaptic neurons.

Peak amplitude of EPSPs and IPSPs was estimated from the average of ≥10 successes. The rise times of synaptic potentials were calculated from onset to peak response. All connections were tested using paired 10 ms pulses separated by 60 ms. The same interval was used to measure short-term plasticity. Paired-pulsed ratio was estimated from failure rates.

Estimating the expected frequencies of polysynaptic circuit motifs. We estimated expected motif frequency by first multiplying the probabilities of each connection type, assuming independent connection probabilities, and then summing values from all simultaneous recordings to define the expected incidence of each motif (Song et al., 2005). Expected motif frequency was determined by dividing this number by the total number of each motif type that was possible in all simultaneously recorded groups of neurons. We determined the significance of our reciprocal and divergent circuit motifs using binomial cumulative distribution functions (Song et al., 2005) to determine the probability of finding a value larger than the number of observed motifs. For example, we found four reciprocal connections between mossy cells and hilar interneurons of 114 possible pairings of these two cell types, yielding a mossy cell/hilar interneuron reciprocal motif frequency of 3.5%. The constituent monosynaptic connection frequencies in this motif were 6.1% (7 observed mossy cell-to-interneuron connections of 114 possible) and 14.9% (17 observed interneuron-to-mossy cell connections of 114 possible). Given these monosynaptic connection probabilities, we expected reciprocal mossy cell/interneuron connections to occur with a frequency of 0.92% (1.0 expected in 114 pairings). We conclude that this reciprocal connection motif occurred more frequently than expected with a confidence level of $p = 0.021$ (stated conservatively as $p < 0.05$; binomial $p = 0.92\%$, $n = 114$; likelihood of four or more motifs computed using binomial cumulative distribution).

We estimated the expected frequency of three- and four-cell motifs using Monte Carlo simulations (Press et al., 1992) to replicate the distributions of hilar cell type constellations recorded simultaneously in each experiment. Monosynaptic connections were assigned based on the connection frequencies (Fig. 4*B*) (e.g., 14.9% of mossy cell/interneuron simultaneous recordings were connected with an inhibitory synapse). Expected motif probabilities were estimated from the frequency that the motif occurred in 10^8 simulations using the Mersenne Twister random number generator. The Monte Carlo and binomial methods generated the same estimate of the expected frequency of mossy cell/interneuron reciprocal motifs.

Results

Despite the potential significance of the dentate hilus to memory function (Lisman, 1999) and epilepsy (Sloviter, 1987), little is known about the function of hilar interneurons or the properties of synapses formed by hilar neurons. The absence of functional information about the basic connectivity of the dentate hilus likely relates to both the absence of dense cell body layers (Amaral, 1978) and the frequent spontaneous synaptic responses hilar

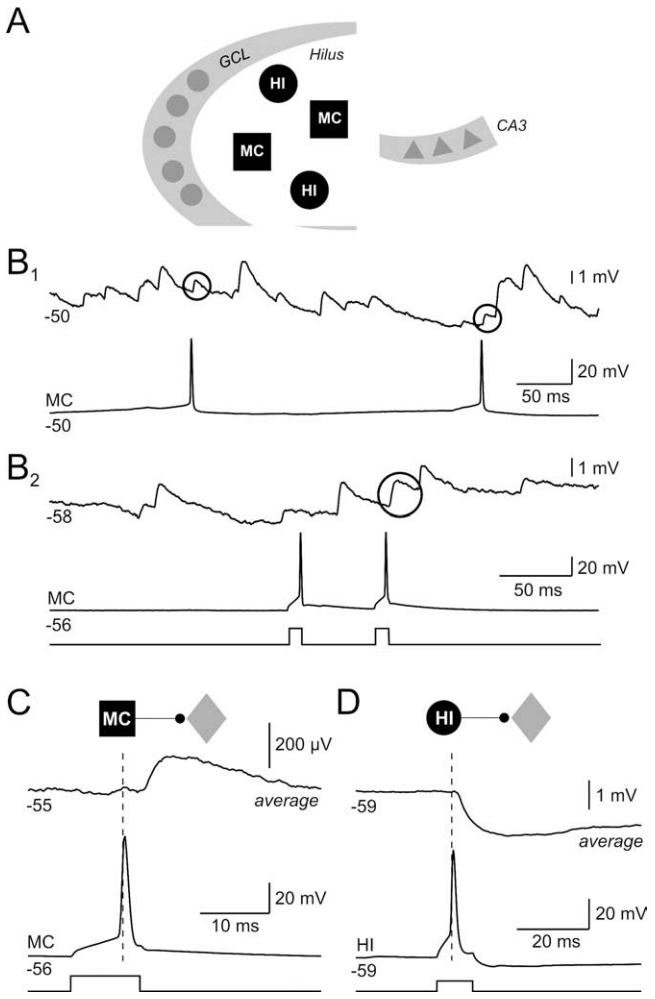

Figure 1. Synaptic connections formed by dentate hilar neurons. ***A***, Schematic representation of the dentate gyrus and CA3 subfield of the hippocampus. The dentate hilus is located between the granule cell layer (GCL) and CA3 and contains primarily two classes of neurons: MCs and HIs. ***B*$_1$**, Paired recording between two hilar neurons. Both spontaneous action potentials in the bottom recording are correlated with EPSPs in the top trace (EPSP onset latencies of 1.8 and 1.6 ms; putative evoked EPSPs enclosed within black circles). ***B*$_2$**, Paired recording between two hilar neurons with one apparent evoked EPSP in the top recording (2.8 ms onset latency) in a different experiment. Both postsynaptic recordings show frequent spontaneous EPSPs that are characteristic of hilar neurons; 400 pA current steps. ***C***, Average postsynaptic response from the paired recording shown in ***B*$_2$** [average of 39 consecutive spike-aligned recordings; paired recording between a mossy cell (black square) and an unclassified hilar neuron (gray diamond)]. ***D***, Average postsynaptic response from a hilar paired recording between an inhibitory interneuron (black circle) and an unclassified hilar cell (average of 31 consecutive spike-aligned episodes); 250 pA current steps.

cells receive in both *in vitro* brain slices (Scharfman, 1993; Strowbridge and Schwartzkroin, 1996) and *in vivo* (Buckmaster et al., 1996). Spontaneous synaptic potentials in hilar neurons greatly increase the difficulty of identifying potential monosynaptic connections in this brain region. Responses to large numbers of precisely timed stimuli are required to verify that apparent postsynaptic responses do not reflect synchronous synaptic input or random coincidences of spontaneous events. The paired recordings in Figure 1*B* illustrate this problem. Putative evoked EPSPs (responses with onset latencies <3 ms, shown within circles) were greatly outnumbered by spontaneous EPSPs that are not correlated with mossy cell spikes. We used an automated *post hoc* procedure in this study to identify synaptic potentials in each record (see Materials and Methods) and visual inspection of

spike-aligned response averages to circumvent this problem, enabling monosynaptic responses evoked between hilar neurons to be defined for the first time.

We tested for synaptic connections among 258 hilar neurons in 35 paired, 44 triple, and 14 quadruple simultaneous intracellular recordings in acute rat hippocampal slices. We recorded postsynaptic responses to presynaptic action potentials evoked by two-pulse stimuli (Fig. 1B_2) in 502 potential hilar synaptic connections. Both individual event detection methods and average trace analysis (see Materials and Methods) identified the same 9 excitatory and 22 inhibitory synaptic connections, including the excitatory connection shown in Figure 1*C* (spike-aligned average response from the same paired recording shown in Fig. 1B_2) and the inhibitory connection shown in the average postsynaptic response in Figure 1*D*. All recordings in this study were performed under current-clamp conditions to enable the intrinsic physiology of both presynaptic and postsynaptic neurons to be assessed (see below) and to facilitate testing for multiple synaptic connections between groups of neurons within the same episode using staggered sets of current pulses.

Synaptic responses of hilar neurons

Figure 2A_1 illustrates a typical excitatory synaptic connection in the hilus and is one one-half of a mossy cell/hilar interneuron reciprocal synaptic connection. Single spikes in this presynaptic mossy cell triggered monosynaptic (<3 ms onset latency) EPSPs with a success rate of 38.4%. The distribution of EPSP amplitudes for this connection had one peak and was skewed toward small-amplitude responses (Fig. 2*B*, left). The mean amplitude of EPSPs in this synapse was 1.06 ± 0.10 mV, measured at −56 mV. The distribution of EPSP onset latencies in this synapse (Fig. 2*C*, left) also had one peak, at 1.87 ± 0.08 ms, consistent with a monosynaptic connection. Figure 2*D*, *E* (red symbols) shows summary data for the amplitudes and latencies of all 9 mossy cell-evoked EPSPs identified in this study. The mean EPSP amplitude was 0.89 ± 0.11 mV and ranged from 0.67 to 1.64 mV. The average mossy cell-evoked EPSP rise time was 3.06 ± 0.22 ms. Mossy cell-evoked EPSPs appeared to be monosynaptic (Doyle and Andresen, 2001) based on their short onset latency (mean 2.00 ± 0.13 ms; range 1.5–2.5 ms; $n = 9$ connections) and low latency jitter (0.46 ± 0.08 ms). We also found no correlation between onset latency and latency jitter ($R^2 = 0.0125$) for mossy cell-evoked EPSPs; such a correlation would be expected if this dataset contained both monosynaptic and longer latency disynaptic responses with increased jitter. Mossy cell synapses have high failure rates (0.79 ± 0.05). The difficulty in detecting monosynaptic excitatory connections reliably during experiments (without *post hoc* data analysis) precluded testing glutamate receptor antagonists on these responses. However, previous studies (Soriano and Frotscher, 1994; Scharfman, 1995; Wenzel et al., 1997) have demonstrated that mossy cells use glutamate as their neurotransmiter. As discussed below, summating mossy cell-evoked EPSPs can reliably trigger APs in postsynaptic neurons (see Fig. 8*D*), confirming the excitatory nature of these responses.

The inhibitory half of this reciprocal mossy cell/hilar interneuron synapse is shown in Figure 2A_2. This connection had a mean amplitude of −1.10 ± 0.04 mV at −60 mV and was highly reliable (9.5% failure rate). Like mossy-cell-evoked EPSPs, the amplitude distribution of IPSPs generated by hilar interneurons had a single peak that was skewed toward small-amplitude events (Fig. 2*B*, right). This inhibitory synapse appeared to be monosynaptic based on its low failure rate and short onset latency

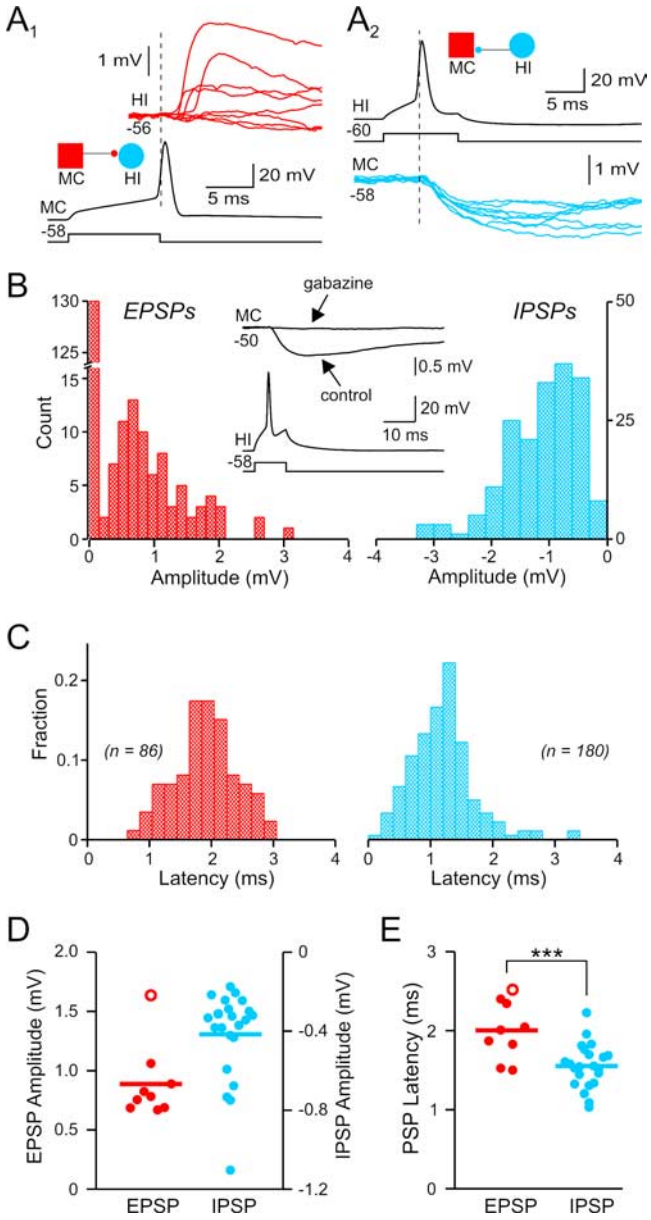

Figure 2. Monosynaptic connections between mossy cells and hilar interneurons. ***A*****$_1$**, Monosynaptic EPSPs evoked by single APs in the MC. Eight consecutive HI postsynaptic responses (shown in red) including four failures. ***A*****$_2$**, Eight consecutive monosynaptic IPSPs (blue traces) recorded in the mossy cell and evoked by single APs in the interneuron. Same mossy cell and interneuron pair in ***A*****$_1$** and ***A*****$_2$**. ***B***, Distribution of unitary EPSP (red) and IPSP (blue) amplitudes in the reciprocal pair shown in ***A***. The failure rate was 62.6% for the EPSP and 9.5% for the IPSP. Inset shows average postsynaptic response before and after bath application of 10 μM gabazine in the same paired recording. ***C***, Distribution of EPSP and IPSP onset latencies from the reciprocal pair shown in ***A***. ***D***, Summary of unitary EPSP (red) and IPSP (blue) amplitudes from 9 excitatory and 22 inhibitory connections. ***E***, Summary of onset latencies from all monosynaptic hilar connections identified. Hilar IPSP onset latencies are significantly shorter than EPSPs (***$p < 0.001$). Open red circles in ***D*** and ***E*** represent values from the one mossy cell-to-mossy cell connection identified; filled red circles represent values from postsynaptic responses in hilar interneurons.

(1.21 ± 0.04 ms; Fig. 2*C*, right). Overall, hilar interneuron-evoked IPSPs had a mean amplitude of −0.42 ± 0.05 mV at −60 mV ($n = 22$ connections) (Fig. 2*D*, blue symbols) and reversed polarity at −76.7 ± 3.8 mV, suggesting that these responses are mediated by $GABA_A$ receptors. We confirmed this in three paired recordings by blocking AP-evoked IPSPs with gabazine (10 μM; Fig. 2*B*, inset). Hilar interneuron-evoked IPSPs had a slower rise

time (4.93 ± 0.26 ms) than mossy cell-evoked EPSPs (significantly different, $p < 0.0001$). All inhibitory connections we identified appeared to be monosynaptic based on their short latencies (mean 1.55 ± 0.06 ms; range 1.0–2.2 ms; significantly shorter than mossy cell-evoked EPSPs; $p < 0.001$; Fig. 2*E*, blue symbols) and low latency jitter (0.27 ± 0.03 ms). Hilar IPSPs had significantly lower failure rates (0.46 ± 0.04) than mossy cell evoked-EPSPs ($p < 0.001$).

Postsynaptic targets of mossy cells and hilar interneurons

Next, we defined the phenotype of the synaptic targets of mossy cells and hilar interneurons to determine the frequency of mossy cell-to-mossy cell, mossy cell-to-interneuron, interneuron-to-mossy cell, and interneuron-to-interneuron connections. The phenotype of the target cell was known in 30% of the monosynaptic connections we identified because that neuron made a reciprocal synapse, such as the example in Figure 2*A*, or synapsed onto another neuron in a simultaneous triple or quadruple recording. We used differences in intrinsic properties to define the postsynaptic targets in the remaining 70% of hilar connections. As illustrated in Figure 3*A*, "known" (i.e., cells that originated one or more identified monosynaptic connections) mossy cells and hilar interneurons generated distinctive responses to depolarizing current steps. Mossy cells tended to respond with an initial burst and, on average, more APs in the first half of the step response (mean spike time = 0.38 ± 0.06; step duration of 4.6 s normalized to 1). In contrast, known hilar interneurons generated APs throughout the step response (mean spike time = 0.54 ± 0.03; significantly different from mossy cells, $p < 0.05$) (Fig. 3*B*, left). Hilar interneurons fired APs in clusters, as indicated by their larger "spike clustering fraction" (0.98 ± 0.01) than mossy cells (0.51 ± 0.11; $p < 0.0001$) (Fig. 3*B*, center) (Dekhuijzen and Bagust, 1996). On average, individual APs in hilar interneurons also triggered more pronounced AHPs than APs in mossy cells [hilar interneuron (HI) AHP slope = 0.459 ± 0.069 vs 0.082 ± 0.020 mV/ms in MCs; $p < 0.001$] (Fig. 3*B*, right). Known mossy cells and hilar interneurons also differed significantly in their membrane time constant (MCs, 22.4 ± 2.5 ms; HIs, 12.4 ± 1.6 ms; $p < 0.05$), capacitance (MCs, 207 ± 32 pF; HIs, 116 ± 12 pF; $p < 0.05$), and AP width (MCs, 2.6 ± 0.1 mV; HIs, 1.8 ± 0.1 mV; $p < 0.001$). Input resistance (MCs, 120 ± 20 MΩ; HIs, 113 ± 11 MΩ) and AP threshold (MCs, −41.3 ± 1.8 mV; HIs, −39.1 ± 1.4 mV) did not differ significantly between known mossy cells and hilar interneurons ($p > 0.05$). The degree of membrane potential sag in responses to hyperpolarizing steps was highly variable in both hilar cell populations and was not analyzed quantitatively.

We found no one parameter that accurately classified hilar cells. However, a simple planar surface using the three intrinsic parameters in Figure 3*B* separated all known mossy cells from hilar interneurons in our dataset (Fig. 3*C*) (see Materials and Methods for details). The categorization of hilar cells into two principal groups is supported by unsupervised k-means cluster analysis. Dividing hilar cells into two groups produces a larger incremental decrease in distortion rate ("jump statistic"; Sugar and James, 2003) than treating all hilar cells as one group or positing three groups. We performed two additional analyses to validate this mossy cell/hilar interneuron separation method. First, we trained a "soft margin", linear kernel support vector machine (Cortes and Vapnik, 1995) on the known data set and found that it classified all hilar neurons ($n = 270$) with <1% discordance from the classification based on the plane in Figure 3*C*. Second, we generated single-plane classifiers using half of the known neurons (all possible combinations of 50% of the known mossy cells and interneurons). These planes correctly classified the remaining half of the known hilar cells (<1.5% discordance) and classified all hilar neurons with a high degree of accuracy (3.2% cells with discordant classifications; 270 cells). These analyses suggest that the hilar neurons in our data set can be reliably classified as mossy cells or hilar interneurons by linear separators based on intrinsic physiology and that this method is not greatly affected by the particular subset of neurons used for training.

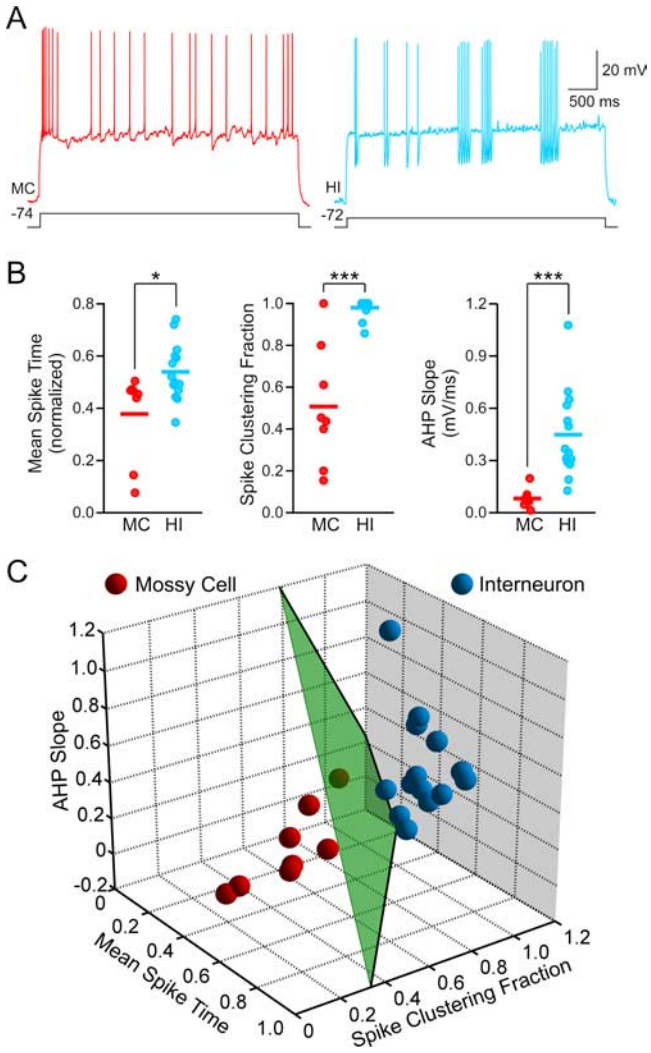

Figure 3. Mossy cells and hilar interneurons can be distinguished by their intrinsic properties. ***A***, Responses to depolarizing steps in a MC that evoked an EPSP in a paired recording (left trace, red) and in a HI (right trace, blue) that evoked an IPSP. Mossy cells typically fire a burst at the beginning of the response and then generate single APs with small AHPs at irregular intervals, whereas hilar interneurons tend to fire intermittent clusters of APs with prominent AHPs. ***B***, Mossy cells have a significantly smaller mean AP time (*$p < 0.05$), smaller spike clustering fraction (***$p < 0.001$), and smaller spike AHP slope (***$p < 0.001$) than hilar interneurons. ***C***, Mossy cells (red spheres; $n = 8$) and interneurons (blue spheres; $n = 14$) can be distinguished by using all three metrics. All three axes reflect the same metrics and units as the plots in ***B***. Separation plane shown in green.

Figure 4*A* shows the bimodal distribution of 270 hilar neurons (258 cells analyzed for synaptic connections and 12 single-cell recordings) based on distance from the separation plane in Figure 3*C*. The mean separation metric of known mossy cells (1.54 ± 0.19; log distance to plane; solid red circles above histogram) closely matched the positive peak of the distribution (1.30) whereas the separation metric of known interneurons (−1.31 ±

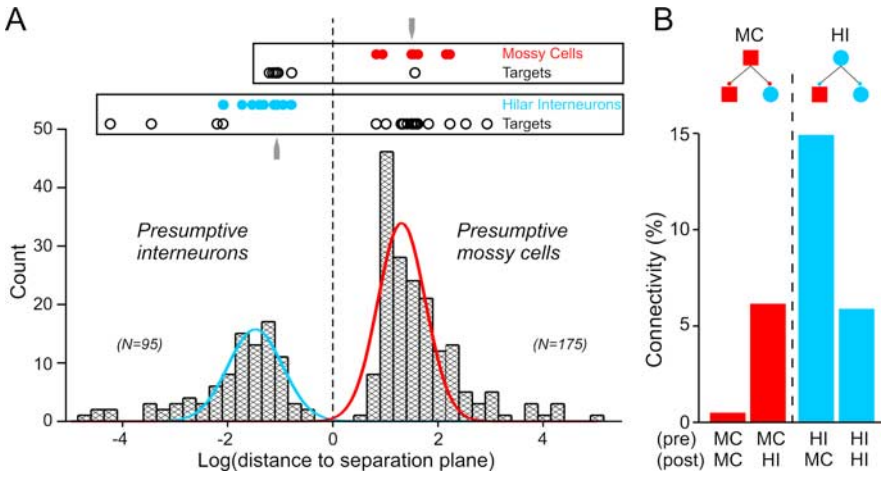

Figure 4. Mossy cells selectively innervate hilar interneurons. ***A***, Analysis of 270 hilar neurons based on distance from separation plane shown in Fig. 3*C* reveals a bimodal distribution. Hilar neurons with positive distance metrics are classified as "presumptive mossy cells" and those with negative metrics as "presumptive interneurons." Filled red and blue circles represent distance metrics for known mossy cells and hilar interneurons, respectively. Distance metrics for postsynaptic targets of known mossy cells and interneurons indicated by open circles. Gray arrows indicate distance metrics of the known mossy cell and hilar interneuron presented in Fig. 2*A*. ***B***, Summary plot of the frequency of the four possible mossy cell/interneuron connection types. We found 1 of 206 possible mossy cell-to-mossy cell connections, 7 of 114 possible mossy cell-to-interneuron connections, 17 of 114 possible interneuron-to-mossy cell connections, and 4 of 68 possible interneuron-to-interneuron connections.

0.12; solid blue circles above histogram) corresponded closely to the negative distribution peak (−1.47). Nearly all hilar cells fell within these two nonoverlapping peaks. We, therefore, termed hilar cells with positive separation distances "presumptive mossy cells" ($n = 175$) and cells with negative distances "presumptive interneurons" ($n = 95$). We also used linear discriminant analysis (Ma et al., 2006) to identify a separation plane for this dataset. This method generated essentially the same separation plane (1% discordant cells) and metrics for individual neurons that were highly correlated with those shown in Figure 4*A* ($R^2 = 0.986$ for the 267 concordant hilar cells).

We next tested this classification scheme by comparing a series of intrinsic properties in the populations of presumptive mossy cells and hilar interneurons. We found that hilar neurons classified as presumptive mossy cells and as presumptive interneurons differed in three other intrinsic parameters that distinguished known mossy cells and interneurons but were not used to generate the separation plane in Figure 3*C* (membrane time constant in presumptive MCs, 26.7 ± 1.1 ms vs 20.6 ± 1.3 ms in HIs, $p < 0.01$; membrane capacitance in MCs, 218 ± 8 pF vs 169 ± 11 pF in HIs, $p < 0.01$; AP width in MCs, 2.8 ± 0.1 ms vs 2.3 ± 0.1 ms in HIs, $p < 0.001$; all differences in the same direction in known and presumptive groups). The parallel differences we found in the independent intrinsic properties between known and presumptive hilar cell groups suggest that the classification metric shown in Figure 4*A* accurately classifies mossy cells and hilar interneurons.

We used this intrinsic classification metric to determine the phenotype of the postsynaptic target cells of known mossy cells and hilar interneurons. We found that mossy cells exhibit remarkable synapse selectivity: nearly all known mossy cells (87.5%) synapsed exclusively onto hilar interneurons, and only one mossy cell synapsed onto another mossy cell. Known hilar interneurons also showed high synapse selectivity and primarily contacted mossy cells (81% of inhibitory connections) with relatively few (19%) connections onto other hilar interneurons; we never observed hilar interneurons that contacted mossy cells and not other interneurons. Distance metrics for postsynaptic targets of known mossy cells and hilar interneurons are plotted within the rectangles in Figure 4*A* (open circles). The summary plot in Figure 4*B* shows the number of the different types of monosynaptic hilar cell connections we observed, normalized by the number of potential connections of that type. We found 6.1% of mossy cell/interneuron pairs had an excitatory connection and 14.9% had an inhibitory connection. Mossy cells formed connections onto other mossy cells very rarely (0.5% connection probability; the one pair shown in Fig. 8*A*; 206 possible mossy cell-to-mossy cell synapses). Hilar interneurons also contacted each other relatively infrequently (5.9% connection probability).

These results suggest that hilar neurons do not randomly innervate other hilar cells: mossy cells preferentially target hilar interneurons and hilar interneurons primarily inhibit mossy cells. It is unlikely that these nonrandom connection patterns reflect a selection bias for slices with less axon truncation because we observed the same rank order of connection probabilities (interneuron-to-mossy cell>mossy cell-to-interneuron>interneuron-to-interneuron>mossy cell-to-mossy cell) when we restricted our analysis to slices with proven monosynaptic connections (i.e., slices with at least one connected pair). We also recorded from 10 hilar cells that formed at least one monosynaptic connection in a simultaneous triple or quadruple recording that included both types of potential target neurons. We observed the same target cell preference in these neurons as we reported in the entire data set (more mossy cell-to-interneuron and interneuron-to-mossy cell connections than expected). Whereas neurons recorded in brain slices obviously have different degrees of axon truncation, variation at the level of individual cells cannot explain nonrandom local connection preferences because this factor will impact all potential connection probabilities equally.

Repeated local circuit motifs in the dentate hilus

The findings presented in Figure 4 demonstrate that hilar neurons do not interconnect randomly but, instead, have preferred target cell types. In addition, we found that multiple structured circuit motifs exist in the hippocampus that involve two or more connections and that these circuit motifs are significantly enriched in the dentate hilus. One common motif we observed was reciprocal connections between mossy cells and hilar interneurons, as illustrated in Figure 2*A*. We found four reciprocal mossy cell/interneuron synapses in our data set: the two sets of reciprocal synapses with a shared interneuron in the quadruple simultaneous recording shown in Figure 5*A*, the reciprocal connection shown in the triple recording in Figure 5*B*, and the paired recording in Figure 2*A*. More than half (57%) of the mossy cell-to-interneuron connections we identified were part of reciprocal synapses. The overall frequency of mossy cell/interneuron reciprocal synapse motifs was significantly greater than expected, given the frequency of each constituent synapse (1.0 reciprocal synapse expected, 4 observed; $p < 0.05$; Fig. 5*C*) (see Materials

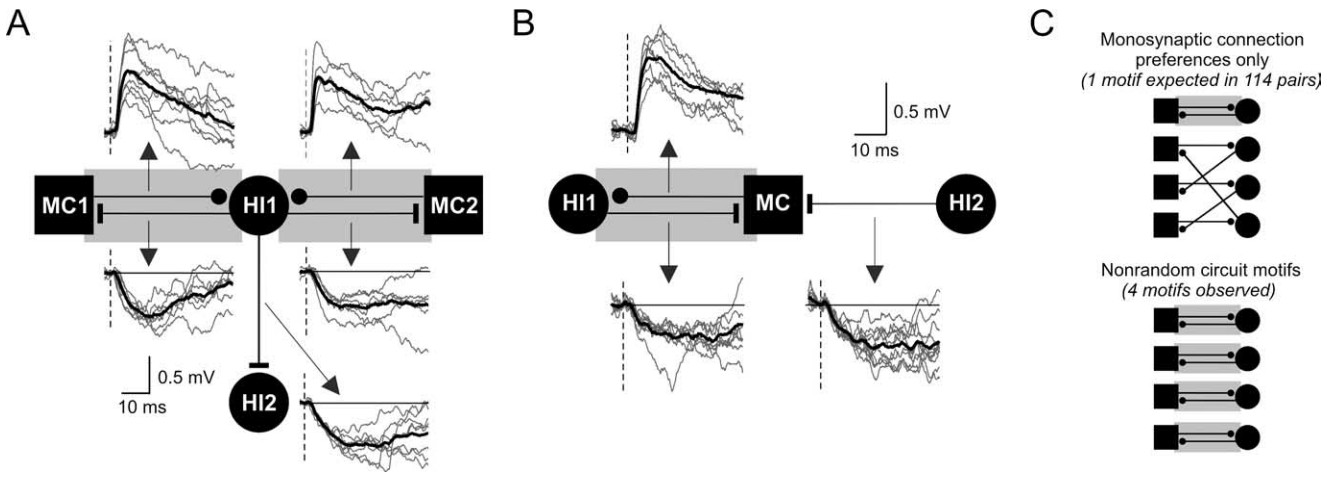

Figure 5. Structured polysynaptic local circuit motifs in the dentate hilus. ***A***, Simultaneous quadruple hilar cell recording with five monosynaptic connections, including two reciprocal mossy cell/interneuron connections (gray rectangles). Recordings also illustrate excitatory synaptic convergence (MC1 and MC2 both excite HI1; EPSP onset latencies = 2.1 and 1.5 ms, respectively) and inhibitory divergence (HI1 inhibits MC1, MC2, and HI2; latencies, 1.7, 1.8, and 2.0 ms). All known phenotypes except HI2 (distance metric, −4.23). Average postsynaptic response shown in bold trace superimposed on example unitary responses (gray traces). Vertical dashed lines indicate presynaptic AP timing (middle of rising phase). ***B***, Simultaneous triple hilar cell recording demonstrating inhibitory convergence (HI1 and HI2 both inhibit MC; IPSP onset latencies, 2.4 and 1.8 ms) and a reciprocal mossy cell/interneuron connection (EPSP onset latency, 1.8 ms). All known phenotypes. ***C***, Diagram representation of hilar circuitry expected on the basis of monosynaptic connection preferences alone (MC/HI reciprocal motif frequency expected = 0.9%; 1 in 114 pairs; top) and observed enrichment of reciprocal motifs in the dentate hilus (observed motif frequency = 3.5%; $p < 0.05$; binomial cumulative distribution; bottom).

and Methods for details). These repeated circuit motifs cannot be explained by proximity because pairs of connected hilar cells were separated by slightly greater intersoma distances (30.7 ± 8.7 μm) than unconnected pairs (26.5 ± 1.7 μm; not significantly different; $p > 0.05$). Our results suggest that networks of hilar neurons are not organized solely on the basis of the monosynaptic connection probabilities. Instead, the hilus contains structured polysynaptic circuits that enable mossy cells to selectively form synapses with "partner" interneurons within a larger population of nearby hilar cells. The frequency of inhibitory divergence (7.5%; Fig. 5*A*) was significantly greater than expected, given the underlying monosynaptic connection probabilities ($p < 0.001$). We also observed excitatory convergence (Fig. 5*A*) and inhibitory convergence (Fig. 5*B*), however these motifs were not statistically enriched in our dataset.

The degree of inhibitory divergence in the dentate hilus was especially striking. Six of 69 (8.7%) hilar interneurons recorded simultaneously with two or more potential target cells generated divergent monosynaptic inhibitory connections. This high frequency of inhibitory divergence was unexpected from the monosynaptic inhibitory connection frequency (14.9%; 2.2% divergent IPSP connection frequency expected). The abundant inhibitory divergence we find in the dentate hilus likely plays an important role in regulating mossy cell excitability and may also help synchronize subpopulations of hilar neurons. We never observed hilar interneurons that selectively targeted other interneurons; all hilar interneurons we identified that inhibited other interneurons also inhibited simultaneously recorded mossy cells (0 interneuron-to-interneuron/mossy cell motifs expected, 4 observed; probability of observing 4 motifs given the monosynaptic connection frequencies was $<10^{-4}$). Individual synapses formed by one hilar interneuron could have very different failure rates. Three of eight pairs of divergent inhibitory connections had failure rates that differed by ≥0.2 and the synapses generated by one divergent connection differed by 72.6% (average difference from the mean failure rates of the identified connections made by that interneuron; 0.63 and 0.10 for this cell). Over the population of eight divergent inhibitory connections, failure rates of synapses from the same interneuron differed by 23.2 ± 8.2%.

Morphology of presumptive mossy cells and hilar interneurons

We next asked how the results of our categorization based on intrinsic physiology correlated with hilar cell morphology. The large number of intracellular recordings attempted in each slice precluded visualizing hilar cell morphology using intracellular dyes in paired recording experiments. Instead, we conducted parallel experiments using slices in which only one cell was recorded and filled with Alexa488 dye through the patch pipette. We used two-photon microscopy to image nine hilar cells classified as mossy cells (mean distance metric = 1.20 ± 0.11) and six hilar interneurons (distance metric = −1.65 ± 0.30). All nine visualized mossy cells were multipolar neurons (4.1 ± 0.4 primary dendrites) (Fig. 6*A*). Axons and dendrites of six of nine mossy cells were well filled and could be assessed for fine morphological characteristics. All six of these mossy cells had thorny excrescences on their proximal dendrites, consistent with previous mossy cell studies (Amaral, 1978; Scharfman and Schwartzkroin, 1988), and conventional spines on distal dendrites (Fig. 6*A*, inset). Axons of well filled mossy cells emerged from the middle of the cell body region (avoiding the somatic poles; five of six cells) and branched extensively within the hilus (Fig. 6*A*, arrows). No filled mossy cell had polarized dendrites similar to those found in granule cells (Amaral, 1978; Claiborne et al., 1990). These anatomical results confirm that the excitatory hilar neurons in our dataset were mossy cells.

Visualized hilar interneurons (Fig. 6*B*) were multipolar (3.2 ± 0.7 primary dendrites) and had similar cell body shape (13.5 ± 0.9 μm width, 23.9 ± 1.4 μm length, shape factor = 1.8) to mossy cells (14.6 ± 0.6 μm width, 22.4 ± 0.8 μm length, shape factor = 1.5; no comparison significantly different; $p > 0.05$). Cell body area also was similar between hilar interneurons (253 ± 22 μm^2) and mossy cells (258 ± 19 μm^2; not significantly different; $p > 0.05$). We examined dendritic and axonal structure in the four hilar interneurons that appeared to be completely filled. Dendrites of all four of these interneurons were sparsely spiny and lacked thorny excrescences found in mossy cells. Axons of hilar interneurons tended to emerge from a somatic pole (4 of 4 interneurons) and branched extensively within the hilus (Fig. 6*B*,

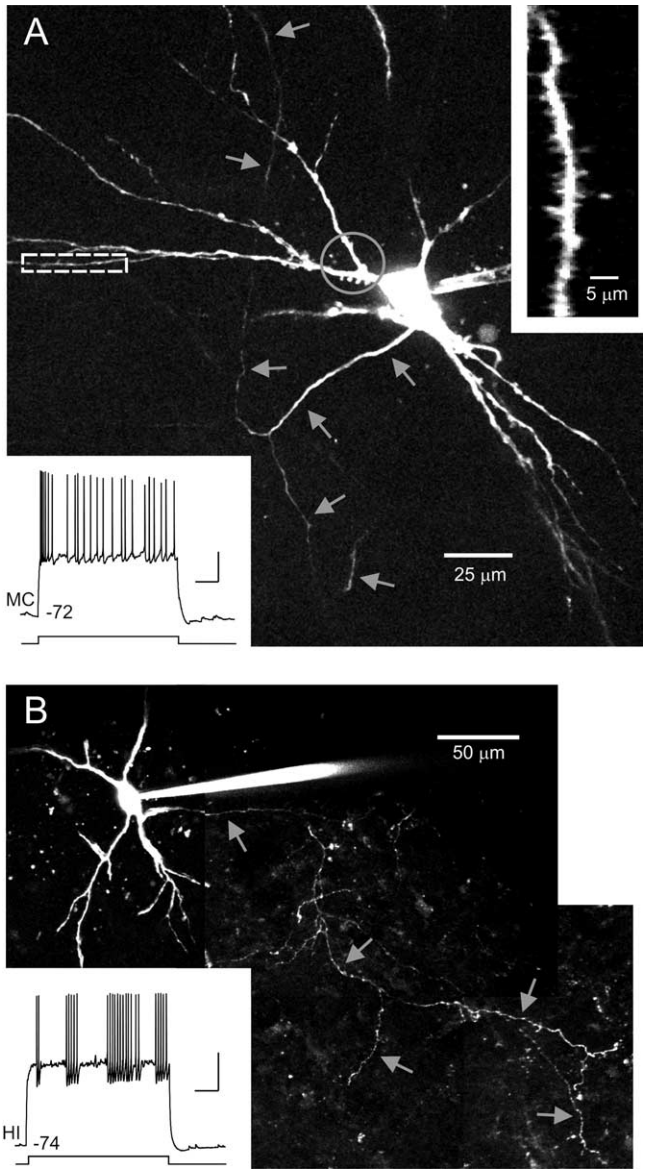

Figure 6. Morphology of hilar neurons. ***A***, Morphology of intracellularly filled mossy cell. Montage of maximal projections from Z-stacks acquired through two-photon imaging of a live brain slice. Gray arrows indicate axonal processes. Enlargement of distal dendrite segment shown in right inset. Enlarged area indicated by white dashed rectangle in main image. Gray circle indicates proximal dendritic segments with thorny excrescences. Bottom inset shows example response of neuron to 3 s depolarizing step (350 pA). Distance metric, 1.04. ***B***, Morphology of filled hilar interneuron. Gray arrows indicate axonal processes. Bottom inset shows example response of interneuron to a 200 pA depolarizing step. Distance metric, −1.31. Calibration: 20 mV, 500 ms (both insets).

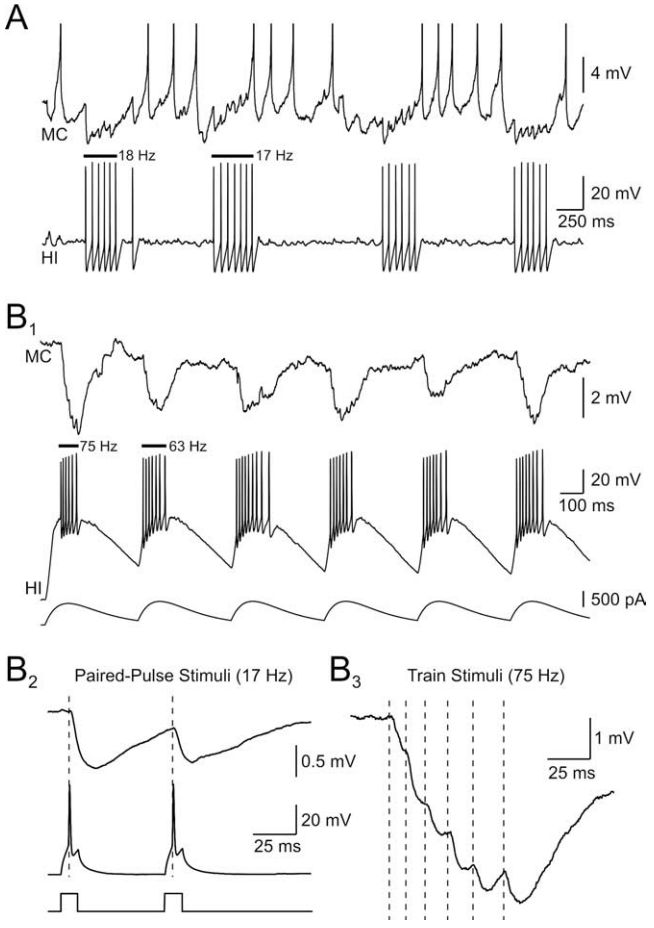

Figure 7. Functional effects of inhibitory hilar synapses. ***A***, Spontaneous discharges in a depolarized hilar interneuron transiently inhibit a postsynaptic mossy cell. Interneuron discharges are correlated with pauses in the mossy cell spontaneous firing. Mean firing frequencies for the initial two interneuron discharges are shown above the recording. Mossy cell action potentials truncated. ***B_1***, Large-amplitude, summating IPSPs evoked by high-frequency hilar interneuron discharges. Interneuron activated by trains of α-function current waveforms. ***B_2***, Unitary IPSPs depress with paired-pulse stimuli (60 ms interval). ***B_3***, IPSPs evoked by high-frequency interneuron bursts summate. Same paired recording in ***B_1–B_3***. Vertical dashed lines indicate timing of action potentials in the presynaptic interneuron driven by an α function current stimulus. The mean presynaptic firing frequency in response to this stimulus was 75 Hz.

arrows) both commonly reported characteristics of hilar interneurons (Lübke et al., 1998). Hilar interneuron axon collaterals formed numerous varicosities, consistent with *en passant* synapses. The absence of basket-like axon segments (Lübke et al., 1998; Acsády et al., 2000) in these neurons (0 of 4 interneurons) suggests that the inhibitory hilar neurons sampled in this study were not basket cells.

Functional properties of hilar synapses

Hilar interneurons frequently generated clusters of APs separated by long (>100 ms) pauses when held at depolarized membrane potentials (Fig. 3*A*). We found that spontaneous AP clusters in hilar interneurons could transiently suppress firing in depolarized postsynaptic mossy cells (Fig. 7*A*). This postsynaptic functional effect appeared to reflect inhibitory shunting because individual IPSPs failed to summate at low firing frequencies (20–40 Hz within AP clusters; Fig. 7*A*). Temporal summation did occur when hilar interneurons were driven strongly by α-function current waveforms (Fig. 7B_1). This stimulus protocol effectively triggered high-frequency presynaptic firing (>60 Hz) that evoked complex IPSPs in target cells that were larger than IPSPs elicited by single APs at the same membrane potential. Large-amplitude summating IPSPs could be evoked repetitively using trains of α-function waveforms ($n = 8$ pairs). Hilar inhibitory synapses depressed when tested with a standard paired-pulse protocol (PPR = 0.86 ± 0.04; 60 ms interval; significantly <1; $p < 0.05$; $n = 22$ connections; Fig. 7B_2). The same inhibitory synapse that depressed with paired stimuli at 17 Hz summated when tested with an α function current stimulus that evoked 75 Hz firing (Fig. 7B_3; presynaptic APs represented by vertical dashed lines). The ability of high frequency IPSPs to summate may reflect the relatively long membrane time constant of mossy cells (22 ms). The

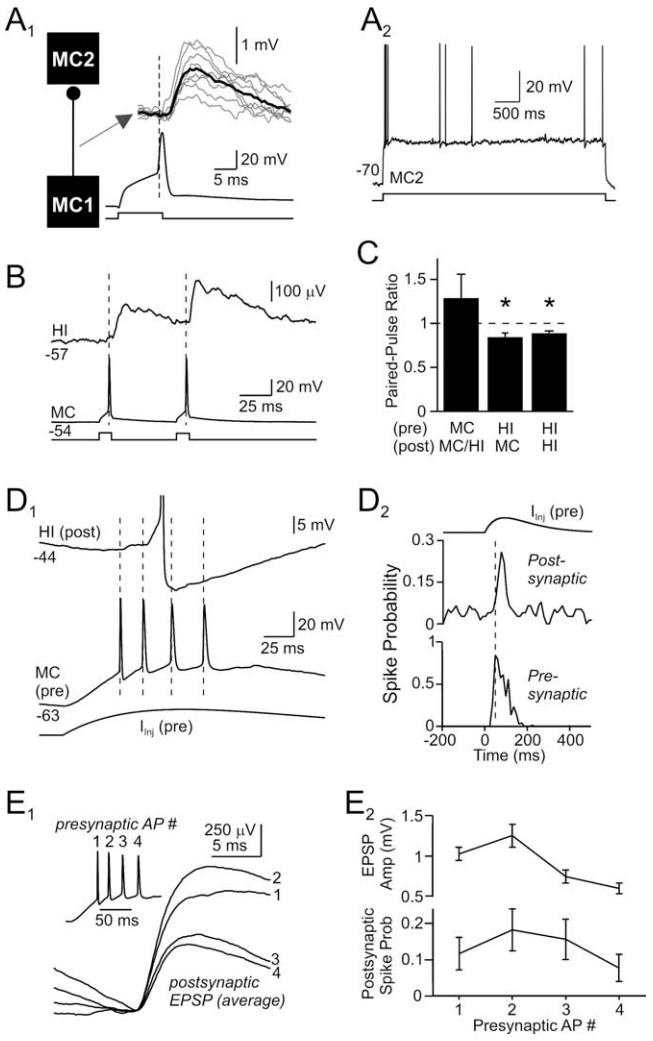

Figure 8. Functional effects of excitatory hilar synapses. ***A*$_1$**, Presumptive mossy cell-to-mossy cell excitatory connection with a mean onset latency of 2.5 ms. Average postsynaptic response shown in bold trace superimposed on example unitary responses (gray traces). ***A*$_2$**, The postsynaptic hilar neuron (distance metric, 1.57; MC2) in this paired recording responded to a depolarizing step with an initial burst followed by irregular spiking and small AHPs, characteristic of mossy cells. ***B***, Averaged postsynaptic response to paired-pulse activation of a mossy cell. Hilar EPSPs showed modest paired-pulse facilitation. ***C***, Summary of short-term plasticity in hilar synapses. Inhibitory responses segregated by phenotype of postsynaptic target; excitatory connections pooled. *$p < 0.05$. ***D*$_1$**, Spike transmission through mossy cell synapses. The presynaptic mossy cell (bottom traces) fired repetitively at ~50 Hz when activated by an α-function current waveform, evoking a series of summating EPSPs and a single AP (truncated) in the postsynaptic hilar interneuron (top trace). ***D*$_2$**, Summary plots of the probability of firing in the presynaptic and postsynaptic cells, versus time, when the presynaptic neuron was driven by trains of α-function current waveforms as in ***D*$_1$**. Repetitive mossy cell firing at 50 Hz reproducibly evoked firing in postsynaptic neurons. ***E*$_1$**, Average spike-aligned responses to the first 4 APs in the α-function-triggered presynaptic bursts. Example presynaptic mossy cell burst shown in inset. The EPSP evoked by the second presynaptic AP was larger than the response to the first AP; subsequent EPSPs were smaller than the initial EPSP response. ***E*$_2$**, Summary plots of EPSP amplitude and postsynaptic spike probability versus presynaptic spike number. Same stimulus protocol as ***D*$_1$** and ***E*$_1$**.

paired-pulse depression observed in this protocol (Fig. 7*B*$_2$) is consistent with the absence of IPSP summation after spontaneous interneuron discharges at similar mean frequencies (Fig. 7*A*). We found no difference in the PPR of inhibitory synapses that related to postsynaptic target cell type (Fig. 8*C*).

Local excitatory synapses generated by mossy cells exhibit high synapse specificity and target almost exclusively hilar interneurons, avoiding other nearby mossy cells (Fig. 4*B*). The one mossy cell-to-mossy cell monosynaptic connection we found is shown in Figure 8*A*$_1$. The phenotype of the target cell is based on intrinsic physiology (distance metric = 1.57; Fig. 8*A*$_2$). This neuron generated a pronounced burst of APs at the beginning of depolarizing steps and did not fire intermittent AP clusters (compare presynaptic interneuron recording in Fig. 7*A*), consistent with established properties of mossy cells (Scharfman and Schwartzkroin, 1988; Buckmaster et al., 1993; Lübke et al., 1998). Unitary EPSPs evoked by this synaptic connection triggered APs when the postsynaptic neuron was held near firing threshold (data not shown). Interestingly, this connection had the largest mean amplitude (1.6 mV) and longest onset latency (2.5 ms) of all nine hilar EPSPs identified (open red circles in Figs. 2*D*,*E*).

In contrast with hilar IPSPs, excitatory hilar synapses facilitated with low-frequency paired-pulse stimulation (mean PPR = 1.29 ± 0.27; 60 ms intervals; $n = 9$ connections, both target phenotypes pooled; Fig. 8*B*,*C*). Mossy cell EPSPs summated when driven by presynaptic AP bursts evoked by trains of α-function current waveforms (Fig. 8*D*$_1$). Action potential bursts in mossy cells could reliably trigger spiking in postsynaptic interneurons held near firing threshold (Fig. 8*D*$_2$). When responses to presynaptic bursts were analyzed per spike, individual EPSPs initially facilitated, then depressed, within the response (Fig. 8*E*$_1$), paralleling the effectiveness of each EPSP in triggering postsynaptic APs (Fig. 8*E*$_2$). Spike transmission was maximal after two presynaptic APs in these responses.

Discussion

This study defines for the first time the synaptic responses evoked by the two major types of dentate hilar neurons (mossy cells and hilar interneurons) and their local connectivity. We find that mossy cells form high failure rate excitatory synapses that facilitate, whereas hilar interneurons generate high-probability synapses that depress with low-frequency paired stimulation. Both mossy cells and hilar interneurons exhibit pronounced target cell selectivity and are frequently connected together through reciprocal local circuit networks. The strong preference for mossy cells to excite interneurons, and interneurons to inhibit mossy cells, may enable hilar networks to generate sparse representations of entorhinal input patterns.

Synapse specificity in the dentate hilus

Because no previous studies have demonstrated unitary synaptic responses evoked by hilar neurons onto local (hilar) targets, the functional organization of this brain region has been inferred through anatomical studies and by correlating morphology with intrinsic properties (Buckmaster et al., 1993; Halasy and Somogyi, 1993; Han et al., 1993; Lübke et al., 1998). The identity of the principal excitatory and inhibitory neurons in the hilus we find, and their intrinsic electrophysiology, correspond well with these previous reports. We find that known excitatory hilar neurons (mossy cells) and hilar interneurons can be distinguished by membrane capacitance, AP width, AP-evoked AHP kinetics and the structure of spiking patterns evoked by depolarizing steps. These characteristics closely match descriptions of the intrinsic electrophysiology of morphologically defined mossy cells (an initial cluster of APs followed by irregular trains of APs with small AHPs) and hilar interneurons (intermittent clusters of APs with pronounced AHPs) reported previously (Scharfman et al., 1990; Buckmaster et al., 1996, 2002; Lübke et al., 1998). Both electrophysiological (Scharfman, 1995) and immunocytochemical studies (Soriano and Frotscher, 1994; Wenzel et al., 1997) have

found that mossy cells are the principal glutamatergic cell type in the hilus. Immunocytochemical studies have revealed a wide variety of hilar interneuronal subtypes (Köhler and Chan-Palay, 1982; Köhler, 1983; Sloviter and Nilaver, 1987), although presumably many interneuronal subclasses share similar intrinsic electrophysiological characteristics. Anatomical studies demonstrated that hilar interneurons tend to densely innervate both local hilar cell processes and granule cell dendritic spines in the outer molecular layer (Mott et al., 1997; Buckmaster et al., 2002). This connection pattern is distinct from dentate basket cells, found typically in the granule cell layer and subgranular zone of the hilus, which primarily inhibit the somata and dendritic shafts of granule cells (Ribak and Seress, 1983; Sik et al., 1997). In addition, the absence of basket-like axonal structures in our intracellularly filled interneurons, and the location of our recordings (in the deep hilus, >80 μm from the granule cell layer), also make it highly unlikely that our dataset included basket cells.

We estimated the local connectivity within the hilus by extending the intrinsic property classification system we developed from known mossy cells and hilar interneurons to include the postsynaptic targets of these cells. We validated our classification system both internally (by statistically comparing alternate classification planes) and externally by examining a constellation of other intrinsic properties that were not used to categorize hilar cells. We found a similarly high degree of synapse specificity (mossy cells tending to excite interneurons and interneurons tending to inhibit mossy cells) in recordings in which intrinsic properties were used to define the postsynaptic target (70% of monosynaptic connections) and the subpopulation of triple and quadruple simultaneous hilar cell recordings in which the phenotype of both presynaptic and postsynaptic neurons were known because they originated monosynaptic connections (30% of connections).

The principal synaptic targets of hilar neurons were subject to disagreement in previous studies. Wenzel et al. (1997) suggested on the basis of ultrastructural methods that mossy cells target other mossy cells and hilar interneurons equally. The high frequency of mossy cell recurrent excitatory connections predicted by that report would help to explain the extreme vulnerability of mossy cells in animal models of epilepsy (Sloviter, 1987) and after repetitive perforant path stimulation *in vitro* (Scharfman and Schwartzkroin, 1990). We find, however, that recurrent connections between mossy cells occur infrequently within the local hilar regions we sampled (<80 μm; 0.5% connection probability). Mossy cells are 13 times more likely to excite nearby interneurons than other mossy cells, in accordance with the anatomical results presented in Buckmaster et al. (1996). The very low frequency of recurrent synapses we find between mossy cells suggests that the dominant intralamellar function of mossy cells is to activate interneurons rather than to propagate or amplify neural activity. The rank order of monosynaptic connection frequency we find also is consistent with the anatomical literature, with generally the strongest evidence for hilar interneuron-to-mossy cell connections (Halasy and Somogyi, 1993; Buckmaster et al., 1996; Sik et al., 1997; Wenzel et al., 1997; Katona et al., 1999; Acsády et al., 2000), followed by mossy cell-to-interneuron synapses (Buckmaster et al., 1996). Our results also show that mossy cell activity can be tightly regulated by hilar interneurons, further limiting the ability of mossy cells to initiate reverberant activity.

Functional significance of reciprocal mossy cell/hilar interneuron synapses

Our recordings demonstrate that reciprocal synapses formed between mossy cells and interneurons occur frequently in the dentate hilus (3.5% of simultaneous mossy cell/hilar interneuron recordings). More than half (57%) of the excitatory mossy cell connections onto hilar interneurons we identified were part of a reciprocal connection with that interneuron. Neither the high degree of synapse specificity of hilar cells nor the frequent reciprocal motifs could be explained by a connection frequency bias toward nearby neurons. Instead, mossy cells appear to preferentially form reciprocal synapses with hilar interneurons, avoiding other nearby mossy cells. We also observed very high frequencies of inhibitory divergence in the hilus; 50% of known interneurons recorded in simultaneous triple or quadruple recordings formed multiple connections. Our results suggest that reciprocal mossy cell/interneuron synapses and divergent inhibitory hilar cell connections are examples of selectively enriched nonrandom polysynaptic circuits. This conclusion parallels a recent study that found statistically enriched nonrandom polysynaptic local circuit motifs in neocortex (Song et al., 2005). Nonrandom local circuits have not been shown previously in the hippocampus or dentate gyrus. Two previous reports described reciprocal excitatory/inhibitory connections in CA1 (Lacaille et al., 1987; Ganter et al., 2004) but neither study found more reciprocal motifs than expected based on individual monosynaptic connection probabilities.

The large variability in IPSP failure rates we found in multiple synapses formed by the same interneuron raises the possibility that inhibitory connectivity may be even higher than demonstrated in this study. If the effectiveness of individual inhibitory connections (e.g., IPSP failure rates) are plastic, the emergence of frequent reciprocal connection between mossy cells and interneurons may reflect activity-dependent upregulation of specific circuit motifs within a dense pattern of axonal interconnections between hilar cells. Future studies correlating patterns of functional interconnections with the frequencies of ultrastructurally defined synapses will be necessary to rigorously test this hypothesis.

Our recordings suggest that hilar interneurons do not simply provide global inhibitory feedback reflecting average mossy cell activity. Instead, the remarkable synapse specificity achieved through mossy cell/interneuron reciprocal connections may enable numerous sparse activity patterns to coexist within the dentate gyrus. Global or randomly connected local inhibitory circuits would tend to extinguish the firing-rate heterogeneity required to generate and maintain sparse representations. Randomly sampling interneurons likely function to scale inputs from other brain regions and prevent input saturation. This adaptive gain control function has recently been demonstrated directly for glomerular-layer interneurons in the insect analog of the olfactory bulb (Olsen and Wilson, 2008). Nonrandom local circuits likely facilitate very different neural computations that depend on separating individual components within complex input patterns. Nonrandom hilar circuit motifs, such as reciprocal excitatory/inhibitory connections, likely achieve gain control across many channels simultaneously, generating orthogonal representations of overlapping input patterns (Rolls and Kesner, 2006). This decorrelating function may be necessary to optimally activate autoassociative networks of CA3 neurons. Recall in these networks is enhanced when they are driven by nonoverlapping input patterns (Marr, 1971). Reciprocal connections between mossy cells and hilar inputs may increase the memory storage

capability of interconnected autoassociative networks by generating sparse intermediate representations of large-scale, overlapping entorhinal input patterns.

This function of hilar local circuits we propose may be functionally related to reciprocal dendrodendritic synapses in the olfactory bulb (Rall et al., 1966; Isaacson and Strowbridge, 1998). Multiple lines of evidence suggest that these local circuits differentiate overlapping input patterns elicited by distinct odorants (Perez-Orive et al., 2002; Assisi et al., 2007; Arevian et al., 2008). Decorrelation of olfactory activity patterns is tightly linked to network oscillations (Perez-Orive et al., 2002), a prominent feature of the dentate gyrus (Csicsvari et al., 2003). Interneurons that form reciprocal connections play an essential role in creating sparse odorant representations by decorrelating stimulus-driven activity patterns (Stopfer et al., 1997; Assisi et al., 2007). We suggest that hilar interneurons may play a similar role in the hippocampus, enabling oscillation-linked sparse hilar cell representations to evolve in response to specific entorhinal input patterns. Because the principal extralamellar synaptic target of mossy cells are granule cells (Buckmaster et al., 1996), sparse hilar cell representations may affect CA3 recall networks by contributing excitatory synaptic input to extralamellar granule cells. In addition, hilar interneurons project widely (Buckmaster et al., 2002), raising the possibility that these GABAergic cells may influence CA3 autoassociative networks directly.

References

Acsády L, Katona I, Martínez-Guijarro FJ, Buzsáki G, Freund TF (2000) Unusual target selectivity of perisomatic inhibitory cells in the hilar region of the rat hippocampus. J Neurosci 20:6907–6919.

Amaral DG (1978) A Golgi study of cell types in the hilar region of the hippocampus in the rat. J Comp Neurol 182:851–914.

Arevian AC, Kapoor V, Urban NN (2008) Activity-dependent gating of lateral inhibition in the mouse olfactory bulb. Nat Neurosci 11:80–87.

Assisi C, Stopfer M, Laurent G, Bazhenov M (2007) Adaptive regulation of sparseness by feedforward inhibition. Nat Neurosci 10:1176–1184.

Buckmaster PS, Jongen-Rêlo AL (1999) Highly specific neuron loss preserves lateral inhibitory circuits in the dentate gyrus of kainate-induced epileptic rats. J Neurosci 19:9519–9529.

Buckmaster PS, Strowbridge BW, Schwartzkroin PA (1993) A comparison of rat hippocampal mossy cells and CA3c pyramidal cells. J Neurophysiol 70:1281–1299.

Buckmaster PS, Wenzel HJ, Kunkel DD, Schwartzkroin PA (1996) Axon arbors and synaptic connections of hippocampal mossy cells in the rat in vivo. J Comp Neurol 366:271–292.

Buckmaster PS, Yamawaki R, Zhang GF (2002) Axon arbors and synaptic connections of a vulnerable population of interneurons in the dentate gyrus in vivo. J Comp Neurol 445:360–373.

Claiborne BJ, Amaral DG, Cowan WM (1990) Quantitative, three-dimensional analysis of granule cell dendrites in the rat dentate gyrus. J Comp Neurol 302:206–219.

Cohen I, Miles R (2000) Contributions of intrinsic and synaptic activities to the generation of neuronal discharges in in vitro hippocampus. J Physiol 524:485–502.

Cortes C, Vapnik V (1995) Support-vector networks. Mach Learn 20:273–297.

Csicsvari J, Jamieson B, Wise KD, Buzsáki G (2003) Mechanisms of gamma oscillations in the hippocampus of the behaving rat. Neuron 37:311–322.

Dekhuijzen AJ, Bagust J (1996) Analysis of neural bursting: nonrhythmic and rhythmic activity in isolated spinal cord. J Neurosci Methods 67:141–147.

Doyle MW, Andresen MC (2001) Reliability of monosynaptic sensory transmission in brain stem neurons *in vitro*. J Neurophysiol 85:2213–2223.

Frazier CJ, Strowbridge BW, Papke RL (2003) Nicotinic receptors on local circuit neurons in dentate gyrus: a potential role in regulation of granule cell excitability. J Neurophysiol 89:3018–3028.

Ganter P, Szücs P, Paulsen O, Somogyi P (2004) Properties of horizontal axo-axonic cells in stratum oriens of the hippocampal CA1 area of rats in vitro. Hippocampus 14:232–243.

Halasy K, Somogyi P (1993) Subdivisions in the multiple GABAergic innervation of granule cells in the dentate gyrus of the rat hippocampus. Eur J Neurosci 5:411–429.

Han ZS, Buhl EH, Lörinczi Z, Somogyi P (1993) A high degree of spatial selectivity in the axonal and dendritic domains of physiologically identified local-circuit neurons in the dentate gyrus of the rat hippocampus. Eur J Neurosci 5:395–410.

Isaacson JS, Strowbridge BW (1998) Olfactory reciprocal synapses: dendritic signaling in the CNS. Neuron 20:749–761.

Katona I, Acsády L, Freund TF (1999) Postsynaptic targets of somatostatin-immunoreactive interneurons in the rat hippocampus. Neuroscience 88:37–55.

Klemm K, Bornholdt S (2005) Topology of biological networks and reliability of information processing. Proc Natl Acad Sci U S A 102:18414–18419.

Köhler C (1983) A morphological analysis of vasoactive intestinal polypeptide (VIP)-like immunoreactive neurons in the area dentata of the rat brain. J Comp Neurol 221:247–262.

Köhler C, Chan-Palay V (1982) Somatostatin-like immunoreactive neurons in the hippocampus: an immunocytochemical study in the rat. Neurosci Lett 34:259–264.

Lacaille JC, Mueller AL, Kunkel DD, Schwartzkroin PA (1987) Local circuit interactions between oriens/alveus interneurons and CA1 pyramidal cells in hippocampal slices: electrophysiology and morphology. J Neurosci 7:1979–1993.

Lisman JE (1999) Relating hippocampal circuitry to function: recall of memory sequences by reciprocal dentate-CA3 interactions. Neuron 22:233–242.

Lübke J, Frotscher M, Spruston N (1998) Specialized electrophysiological properties of anatomically identified neurons in the hilar region of the rat fascia dentata. J Neurophysiol 79:1518–1534.

Ma Y, Hu H, Berrebi AS, Mathers PH, Agmon A (2006) Distinct subtypes of somatostatin-containing neocortical interneurons revealed in transgenic mice. J Neurosci 26:5069–5082.

Marr D (1971) Simple memory: a theory for archicortex. Philos Trans R Soc Lond B Biol Sci 262:23–81.

Morgan RJ, Soltesz I (2008) Nonrandom connectivity of the epileptic dentate gyrus predicts a major role for neuronal hubs in seizures. Proc Natl Acad Sci U S A 105:6179–6184.

Mott DD, Turner DA, Okazaki MM, Lewis DV (1997) Interneurons of the dentate-hilus border of the rat dentate gyrus: morphological and electrophysiological heterogeneity. J Neurosci 17:3990–4005.

Olsen SR, Wilson RI (2008) Lateral presynaptic inhibition mediates gain control in an olfactory circuit. Nature 452:956–960.

Perez-Orive J, Mazor O, Turner GC, Cassenaer S, Wilson RI, Laurent G (2002) Oscillations and sparsening of odor representations in the mushroom body. Science 297:359–365.

Press WH, Vetterling WT, Teukolsky SA, Flannery BP (1992) Numerical recipes in C, Ed 2. Cambridge, UK: Cambridge UP.

Rall W, Shepherd GM, Reese TS, Brightman MW (1966) Dendrodendritic synaptic pathway for inhibition in the olfactory bulb. Exp Neurol 14:44–56.

Ribak CE, Seress L (1983) Five types of basket cell in the hippocampal dentate gyrus: a combined Golgi and electron microscopic study. J Neurocytol 12:577–597.

Rolls ET, Kesner RP (2006) A computational theory of hippocampal function, and empirical tests of the theory. Prog Neurobiol 79:1–48.

Sass KJ, Sass A, Westerveld M, Lencz T, Novelly RA, Kim JH, Spencer DD (1992) Specificity in the correlation of verbal memory and hippocampal neuron loss: dissociation of memory, language, and verbal intellectual ability. J Clin Exp Neuropsychol 14:662–672.

Scharfman HE (1993) Characteristics of spontaneous and evoked EPSPs recorded from dentate spiny hilar cells in rat hippocampal slices. J Neurophysiol 70:742–757.

Scharfman HE (1995) Electrophysiological evidence that dentate hilar mossy cells are excitatory and innervate both granule cells and interneurons. J Neurophysiol 74:179–194.

Scharfman HE, Schwartzkroin PA (1988) Electrophysiology of morphologically identified mossy cells of the dentate hilus recorded in guinea pig hippocampal slices. J Neurosci 8:3812–3821.

Scharfman HE, Schwartzkroin PA (1990) Responses of cells of the rat fascia dentata to prolonged stimulation of the perforant path: sensitivity of hilar cells and changes in granule cell excitability. Neuroscience 35:491–504.

Scharfman HE, Kunkel DD, Schwartzkroin PA (1990) Synaptic connections of dentate granule cells and hilar neurons: results of paired intracellular recordings and intracellular horseradish peroxidase injections. Neuroscience 37:693–707.

Sik A, Penttonen M, Buzsáki G (1997) Interneurons in the hippocampal dentate gyrus: an in vivo intracellular study. Eur J Neurosci 9:573–588.

Sloviter RS (1987) Decreased hippocampal inhibition and a selective loss of interneurons in experimental epilepsy. Science 235:73–76.

Sloviter RS, Nilaver G (1987) Immunocytochemical localization of GABA-, cholecystokinin-, vasoactive intestinal polypeptide-, and somatostatin-like immunoreactivity in the area dentata and hippocampus of the rat. J Comp Neurol 256:42–60.

Song S, Sjöström PJ, Reigl M, Nelson S, Chklovskii DB (2005) Highly nonrandom features of synaptic connectivity in local cortical circuits. PLoS Biol 3:e68.

Soriano E, Frotscher M (1994) Mossy cells of the rat fascia dentata are glutamate-immunoreactive. Hippocampus 4:65–69.

Stopfer M, Bhagavan S, Smith BH, Laurent G (1997) Impaired odour discrimination on desynchronization of odour-encoding neural assemblies. Nature 390:70–74.

Strowbridge BW, Schwartzkroin PA (1996) Transient potentiation of spontaneous EPSPs in rat mossy cells induced by depolarization of a single neurone. J Physiol 494:493–510.

Sugar CA, James GM (2003) Finding the number of clusters in a dataset: an information-theoretic approach. J Am Stat Assoc 98:750–763.

Wenzel HJ, Buckmaster PS, Anderson NL, Wenzel ME, Schwartzkroin PA (1997) Ultrastructural localization of neurotransmitter immunoreactivity in mossy cell axons and their synaptic targets in the rat dentate gyrus. Hippocampus 7:559–570.

Williams PA, Larimer P, Gao Y, Strowbridge BW (2007) Semilunar granule cells: glutamatergic neurons in the rat dentate gyrus with axon collaterals in the inner molecular layer. J Neurosci 27:13756–13761.